A Compressive Sensing Control Matrix Generating Technique to Extend the Field of View for Drone Detection Optical Systems

Hoang Thi Phuong Thao
Faculty of Electronics and Telecommunications, Power University, Hanoi, Vietnam
thaohp@epu.edu.vn (corresponding author)

Nguyen Le Cuong
Faculty of Electronics and Telecommunications, Power University, Hanoi, Vietnam
cuongnl@epu.edu.vn

Tran Vu Kien
Faculty of Electronics and Telecommunications, Power University, Hanoi, Vietnam
kientv@epu.edu.vn

Received: 18 March 2025 | Revised: 2 May 2025 | Accepted: 13 May 2025

 DOI: https://doi.org/10.48084/etasr.11018

ABSTRACT

Detecting drones based on optical images is a popular topic in current research. However, most current optical systems have a narrow Field of View (FoV), so they often combine many cameras into scanning systems to observe a wide area, reducing object detection speed. This paper presents an optical model that applies compressive sensing techniques to capture images from two FoVs using a single 2D image sensor. This work aims to enhance drone detection by improving image capture efficiency, reducing the need for multiple cameras, and improving detection speed. The sampling process utilizes a Digital Mirror Device (DMD) combined with the proposed control technique. The control technique uses a matrix with columns formed from pseudorandom binary sequences generated from primitive polynomials over a finite field through trace functions and D-transforms. After compressed sensing, data recovery is performed using the popular Orthogonal Matching Pursuit (OMP) recovery algorithm. The system can reduce the number of cameras required and increase object detection speed by not using a scanner such as traditional systems. The effectiveness of the proposed model is evaluated based on Peak Signal Noise Ratio (PSNR), Normalized Root Mean Squared Error (NRMSE), and processing time, using simulated data of drone images under various conditions. The simulation results demonstrate the system's effectiveness, with PSNR ranging from 24.52 to 52.39 dB, NRMSE between 0.004 and 0.081, and reduced processing times, validating its feasibility and advantages for real-time wide-FoV optical drone detection.

Keywords-compressive sensing; DMD matrix; detecting drones

I. INTRODUCTION

Recently, the use of drones has increased in many fields, such as commerce, rescue, military, and everyday life. In addition to their benefits, drones can be used for illegal activities, so detecting them is essential for various organizations. Drone detection methods are based on active radar detection [1, 2] and RF (Radio Frequency) [3, 4], acoustic [5-7], and optical [8-10] signals. Drone detection systems that use active radar-based methods to transmit and receive reflected signals to detect objects have advantages such as high accuracy and the ability to be unaffected by environmental conditions. However, active radar-based systems have several limitations, including their high cost and inability to detect small objects. RF signal-based techniques use signals between drones and control stations to detect them. The advantages of this technique are the long detection range and the fact that it is unaffected by lighting conditions. However, noise and obstructions significantly affect drone detection based on RF. Detection systems that use acoustic sensors analyze drone sounds during flight to detect them. This approach is insensitive to lighting conditions, but its detecting accuracy is low in noisy environments, and acoustic sensors cannot detect the presence of drones at long distances.

Optical systems use camera sensors to capture drones and process visual data to detect their positions. These systems are inexpensive and have many algorithms to support visual data processing. These systems serve as suitable options for drone detection in situations where drones emit weak sounds or low

RF signals [8-13]. The systems proposed in [8-10] use camera sensors to capture visual data and then combine artificial intelligence with high system efficiency but a narrow camera FoV. The optical-based drone detection systems in [11, 12] addressed this limitation with improved FoV using audio data collected from drones to alter the camera's monitoring direction. However, these systems still have limitations related to the acoustic method. Additionally, mechanical rotation reduces the speed of detecting and tracking drones. In [13], the FoV of optical systems was improved by employing a single image sensor to capture images from two different FoVs. However, the composite visual data from the two FoVs are reconstructed based on a Convolutional Neural Network (CNN), making the system more complex in hardware and algorithms. In summary, there is a challenge for optical-based drone detection systems to expand FoV while maintaining simple hardware, improved process efficiency, and fast detection speed.

This study presents an optical drone detection system for simultaneously capturing images from two FoVs using the proposed control technique for a Digital Micromirror Device (DMD). The system consists of the following blocks: optical, image sensor, DMD control, and digital processing. The optical system uses the compressive sensing technique to capture images from two directions to achieve a wide FoV. The optical block comprises an image sensor, a DMD, and other optical components. The DMD, composed of tiltable micromirrors arranged in a square matrix, acts as a compressive sensing matrix, each serving as a pixel [14]. The state of each matrix element changes based on the directions of the micromirrors on the DMD and is controlled by the proposed technique, which is performed by Field-Programmable Gate Array (FPGA) digital electronic systems in the control block. The FPGA system generates pseudorandom binary sequences using primitive polynomials in the appropriate order for the column of the DMD matrix [15]. Light from two objects in two FoVs is directed to the DMD and then modulated by the DMD matrix, each having different polarizations due to polarizing beam splitters. The light paths are finally directed toward the image sensor block after going through the additional optical components and two mirrors. These mirrors are placed in two different spatial directions to obtain two submatrices, the parts of the DMD matrix. These submatrices compress the received images, making them smaller than the original ones. The image sensor captures images of both objects simultaneously and then transmits them to the digital processing block. The Orthogonal Matching Pursuit (OMP) [16] recovery algorithm, based on dynamic programming in the digital processing block, takes advantage of polarization-based light separation to restore the original compressed image.

The novelty of this work is that the optical drone detection system can simultaneously capture two distinct FoVs with two lenses but only a single camera using the proposed binary control matrix for a DMD. The matrix is generated using pseudorandom sequences derived from primitive polynomials and enhanced through nonlinear transformations. Unlike traditional sensing matrices (e.g., Gaussian or Bernoulli), the proposed matrix has both ideal incoherence properties and minimal hardware demands. This condition ensures a signal recovery process with minimal recovery error. In addition, the matrix requires very little storage space, low hardware, reduced generating time, and a simple process due to generating primitive polynomials. The benefit of the system is that it can sample two or more objects in a single shot, enhancing the efficiency of data storage and transmission. In addition, it can sample from two different FoVs by using two lenses but only one camera, which addresses the narrow FoV limitation of optical systems without adding more cameras or traditional scanning methods. Two drone images from two FoVs in one shot are compressed into a single drone image. Then, it is reconstructed based on the OMP algorithm in the digital processing block to evaluate the system's feasibility. The simulated Peak Signal-to-Noise Ratio (PSNR) and Normalized Root Mean Squared Error (NRMSE) values range from 24.52 to 52.39 dB and from 0.004 to 0.081, respectively, which meet the criteria for image processing.

II. SYSTEM MODEL

A. System Model for Capturing Images

Figure 1 describes the system model for capturing compressed images from two FoVs. Figure 2 shows details on the optical block.

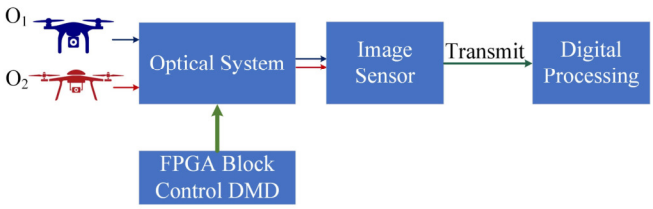

Fig. 1. Model for capturing images from two FoVs.

The optical block consists of lenses (L_1, L_2), Beam Splitters (BS), Polarizing Beam Splitters (PBS_1, PBS_2), an image sensor, a DMD, and two mirrors (M_1, M_2). Light from two sampling objects, O1 and O2, is collected by lenses L1 and L2 and then passes through the PBS1 to create the *p*- and s-polarization states, respectively. Next, part of the composite beam coming to BS is redirected to the DMD, which plays a crucial role in modulating the light. After being modulated by DMD, the light passes through the BS and reaches the PBS2 to split into two different polarized components. These two components are then reflected by mirrors M_1 and M_2. As shown in Figure 3, these mirrors are positioned in two distinct spatial orientations to obtain two submatrices that compress the received pictures to make them smaller than the originals. The image sensor takes photos of both objects simultaneously and sends them to the digital processing block.

B. Mathematical Model

The mathematical model of the system is described as follows. Assume the two drones O_1, O_2. X_1 and X_2 ($X_1, X_2 \in R^{N\times N}$) are images of O_1 and O_2, respectively, which are represented on a spatial plane with $N \times N$ pixels. The light signal after passing the BS is represented by $(X_1 + X_2)$. A portion of $(X_1 + X_2)$ is directed to the DMD and modulated by the matrix Φ as in (1), creating $(X_1 + X_2)$.

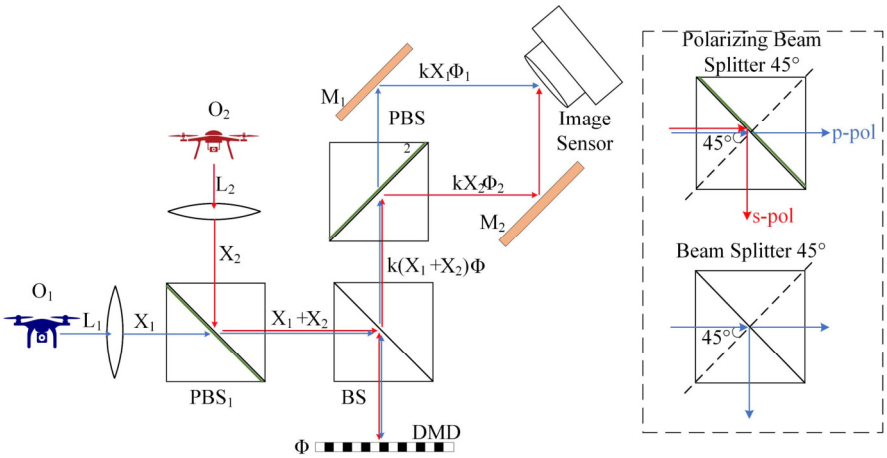

Fig. 2. Working principle of the system.

$$\Phi = \begin{bmatrix} a_{00} & a_{01} & \cdots & a_{0(N-1)} \\ a_{10} & a_{11} & \cdots & a_{1(N-1)} \\ \vdots & \vdots & \ddots & \vdots \\ a_{(N-1)0} & a_{(N-1)1} & \cdots & a_{(N-1)(N-1)} \end{bmatrix} \quad (1)$$

where matrix elements $(a_{ij},\ i = 0, \dots, N-1,\ j = 0, \dots, N-1)$ are the values of the bit in the random sequence used to control the DMD. Based on Φ, compressive sensing submatrices Φ_1 and Φ_2 are created by two mirrors M_1 and M_2. Φ_1 and Φ_2 are part of the Φ matrix, and their row numbers are equal to $\frac{1}{2}N$, which means that the compression factor is equal to 0.5. Φ_1 and Φ_2 are defined as:

$$\Phi_1 = \begin{bmatrix} a_{00} & a_{01} & \cdots & a_{0(N-1)} \\ a_{10} & a_{11} & \cdots & a_{1(N-1)} \\ \vdots & \vdots & \ddots & \vdots \\ a_{(\frac{N}{2}-1)0} & a_{(\frac{N}{2}-1)1} & \cdots & a_{(\frac{N}{2}-1)(N-1)} \end{bmatrix} \quad (2)$$

$$\Phi_2 = \begin{bmatrix} a_{(\frac{N}{2})0} & a_{(\frac{N}{2})1} & \cdots & a_{(\frac{N}{2})(N-1)} \\ a_{(\frac{N}{2}+1)0} & a_{(\frac{N}{2}+1)1} & \cdots & a_{(\frac{N}{2}+1)(N-1)} \\ \vdots & \vdots & \ddots & \vdots \\ a_{(N-1)0} & a_{(N-1)1} & \cdots & a_{(N-1)(N-1)} \end{bmatrix} \quad (3)$$

The input signal to the image sensor $Y \in R^{(\frac{N}{2} \times N)}$ is calculated according to:

$$Y = k.\Phi_1.X_1 + k.\Phi_2.X_2 + \varepsilon \quad (4)$$

where ε is the system's noise and k is the attenuation factor of the DMD.

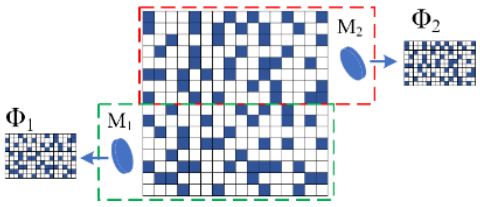

Fig. 3. Method for generating two sensing matrices.

C. Matrix Generation Technique for Controlling the DMD

To successfully perform compressive sensing and reconstruct an image, the original images and the sensing matrix must meet the following conditions [17]:

- The original image must have sparsity in a spatial domain. For drone images in the sky, this property is generally satisfied.
- The sensing matrix must have good incoherence. This property ensures that the matrix can capture sufficient information from the sparse image.
- The sensing matrix must satisfy the Restricted Isometry Property (RIP), ensuring it preserves the non-overlapping and structural properties of significant image components after compression.

Matrices satisfying the above conditions are often random, such as Gaussian or Bernoulli matrices. In practical applications, the Gaussian and Bernoulli matrices typically consume significant resources for both generating matrices and reconstructing images. This paper presents a technique for generating a binary matrix to control the DMD and satisfy the above compressive sensing criteria. The matrix has a bit probability of 0 equal to bit 1, and the cross-correlation value between the columns of the matrix is approximately zero. This matrix requires very low storage space and minimal hardware implementation. The matrix is created using the following steps.

1) Step 1: Generating a Linear Sequence

The proposed matrix size is $N \times N$ with its columns consisting of pseudorandom binary sequences, which are created based on the generating primitive polynomial $g(x)$ in the Galois Field $(GF(2^n))$, $g(x) = x^n + g_{(n-1)}x^{(n-1)} + \cdots + g_1 x + g_0$, with $g_i \in [0, 1]$. The image and matrix sizes are the same, which depend on the polynomial order (n) according to [18]:

$$N = 2^n - 1 \quad (5)$$

The pseudorandom sequence created by $g(x)$ can be implemented by a Linear Feedback Shift Register (LFSR) [19]. The initial LFSR value is described by the $S(0)$ matrix as follows:

$$S(0) = \begin{bmatrix} s_0(0) \\ s_1(0) \\ s_2(0) \\ \vdots \\ s_{n-1}(0) \end{bmatrix} \quad (6)$$

where $s_n(0)$ is the value of the n^{th} bit in the register.

The transition matrix G of LFSR is of size $n \times n$, which describes the shift and feedback process. The matrix G represents the operation of LFSR to generate a bit sequence.

$$G = \begin{bmatrix} 1 & 0 & 0 & \cdots & 0 & 0 \\ 0 & 1 & 0 & \cdots & 0 & 0 \\ 0 & 0 & 1 & \cdots & 0 & 0 \\ \vdots & \vdots & \vdots & \ddots & \vdots & \vdots \\ g_0 & g_1 & g_2 & \cdots & g_{n-2} & g_{n-1} \end{bmatrix} \quad (7)$$

The present state of LFSR at (t) is calculated by multiplying the transition matrix G by the previous state at $(t-1)$:

$$s(t) = G.s(t-1) \quad (8)$$

After N shifts of LFSR, the sequence of output linear bits follows.

$$A_{1\times N} = [s_0(0), s_0(1), s_0(2), \cdots, s_0(N-1)] \quad (9)$$

To enhance the correlation and randomness properties, $A_{1\times N}$ is converted to a nonlinear sequence as in step 2.

2) Step 2: Finding the Position for Interleaving

The sequence $A_{1\times N}$ is transformed into the nonlinear sequence $\{b_n\}$ by interleaving subsequences of m -order primitive polynomial (where m is a divisor of n) into the sequence $A_{1\times N}$. The subsequences are interleaved into the sequence $A_{1\times N}$ at the phase positions I_P^j, calculated through the trace function [20, 21]:

$$I_P^j = \begin{cases} i & if \quad Tr_m^n(s^j) = s^{Ti} \quad i \in [0, 2^m - 1] \\ \infty & if \quad Tr_m^n(s^j) = 0 \quad j \in [0, T] \end{cases} \quad (10)$$

where:

$$Tr_m^n(s) = \sum_{k=0}^{\frac{n}{m}-1} s^{2^{mk}} \quad (11)$$

$$T = \frac{(2^n-1)}{(2^m-1)}.$$

The $A_{1\times N}$ sequence is sampled with interval T and can be arranged as columns of a matrix for easy tracking.

$$A_{(2^m-1)\times T} = \begin{bmatrix} s_0 & s_1 & \cdots & s_{T-1} \\ s_T & s_{T+1} & \cdots & s_{2T-1} \\ \vdots & \vdots & \ddots & \vdots \\ s_{(2^m-2)T} & s_{(2^m-2)T+1} & \cdots & s_{(2^m-1)T-1} \end{bmatrix} \quad (12)$$

From the trace function point of view, it can be seen that the columns of the matrix are the phases of the subsequence.

3) Step 3: Generating a Nonlinear Sequence

The subsequences of m-order primitive polynomial $\left(h(x) = x^m + h_{(m-1)}x^{(m-1)} + \cdots + h_1 x + h_0\right)$ are substituted into the interleaving positions of $A_{1\times N}$ at the phases as in (12). The sequence after substitution is transformed into the nonlinear sequence $\{b_n\}$ based on D-transform as in (13).

$$\{b_n\} = \sum_{i=0}^{T-1} D^i.w_i(D^T), i = 0,1,\cdots,T-1 \quad (13)$$

where:

$$w_i(D) = \frac{s_i(D)}{h_s(D)}, i \in [0, T-1] \quad (14)$$

According to the properties of the D-transformation, the sequence $\{b_n\}$ can be constructed by alternating T phases of $\{w_i\}$. In terms of the D-transformation, this is the time concatenation of $\{w_i\}$.

The nonlinear sequence obtains an ideal auto-correlation characteristic thanks to the interleaved structure based on the I_P^j phase sequence. Moreover, the subsequence replacement ensures the balance of the 0 and 1 bits of the nonlinear sequence, which helps to increase the random properties of the sequence. Performing a circular shift on the sequence $\{b_n\}$, $2^n - 1$ pseudorandom nonlinear sequences are obtained, which are used as columns of the matrix Φ. This matrix Φ is stored as byte data in the FPGA's flash memory. During sampling, the data in the memory is read by a clock pulse and transferred onto the data stream to control the DMD device based on a lookup table mechanism, as shown in Figure 4.

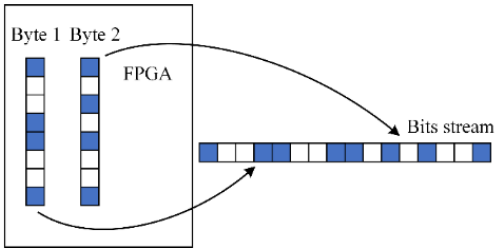

Fig. 4. Generate pseudorandom sequence from hardware.

III. IMAGE RECONSTRUCTION

After compressed sensing, the signal is restored using digital processors or a computer based on recovery algorithms. Several popular algorithms have been proposed, such as MP [22], OMP [16], CoSaMP [23], and BP [24]. This paper uses the OMP algorithm [16] to reconstruct the compressive sensing image, which verifies the performance of the proposed matrix-generating technique. The algorithm works based on Dynamic Programming (DP). It iteratively searches for signal components and terminates the process based on the established conditions for the number of iterations and the residual value. DP-based algorithms have the advantage of low computational complexity. Algorithm 1 shows the OMP algorithmic procedure.

Algorithm 1 Orthogonal Matching Pursuit (OMP)
Input: Measurement matrix Φ_1, Φ_2,
  measurement vector Y,
  number of iterations K
Output: Sparse signal $\hat{X}_1$ and $\hat{X}_2$
Initialize: $\hat{X}_1 = 0$, $\hat{X}_2 = 0$, $\Lambda_1 = \emptyset$, $\Lambda_2 = \emptyset$
For k = 1 to K do
  Find the index i_k, j_k that solves:
  $i_k = arg\ \max_i |\langle \Phi_{1i}, r \rangle|$
  $j_k = arg\ \max_i |\langle \Phi_{2i}, r \rangle|$
  Update the index set
  $\Lambda_1 = \Lambda_1 \cup \{i_k\}$, $\Lambda_2 = \Lambda_2 \cup \{j_k\}$
  State Solve the least squares problem to update $\hat{X}_1$ and $\hat{X}_2$:
  $X_{1\Lambda_1} = arg\ \min_z \left\| Y_1 - \Phi_{1\Lambda_1} z \right\|_2$
  $X_{2\Lambda_2} = arg\ \min_z \left\| Y_2 - \Phi_{2\Lambda_2} z \right\|_2$
  Update the residual:
  $r_1 = Y_1 - \Phi_{1\Lambda_1} \hat{X}_{1\Lambda_1}$
  $r_2 = Y_2 - \Phi_{2\Lambda_2} \hat{X}_{2\Lambda_2}$
  If the stopping criterion is met then:
    break
  End If
End For
Return $\hat{X}_1$ and $\hat{X}_2$

where, Λ_1 and Λ_2 are submatrices formed by the columns of the matrix Φ_1, Φ_2, and $\|.\|_1$ is the ℓ_2-norm [25]. These steps are repeated until the result satisfies the conditions for the number of iterations or the residual value.

IV. SIMULATION RESULTS AND DISCUSSION

The simulation evaluates the DMD control matrix generation technique by comparing it with two popular matrices used for compressive sensing, the Gaussian matrix and the Bernoulli matrix [26]. Drone images converted to grayscale were input data for the simulation process. This simulation was carried out using Python version 3.12, running on an Intel Core i7 NUC computer with 32 GB of RAM.

The model's performance was evaluated using PSNR, NRMSE, and processing time according to (15) and (17). The execution time of the process is measured from the sensing stage to successful image reconstruction.

$$PSNR = 10\, log_{10}\left(\frac{MAX_I^2}{MSE}\right) \quad (15)$$

where MAX_I is the maximum value of a pixel,

$$MSE = \frac{1}{n}\sum(y - \hat{y})^2 \quad (16)$$

NRMSE is used to evaluate the model's accuracy.

$$NRMSE = \frac{\sqrt{\sum(y-\hat{y})^2}}{\sqrt{\sum(y)^2}} \quad (17)$$

where y is the input image, and $\hat{y}$ is the reconstructed image.

In this simulation scenario, the sensing matrix is generated from the 9[th]-order generating primitive polynomial $g(x) = x^9 + x^4 + x^3 + x + 1$ over the field $GF(2^9)$ and on $GF(2^3)$. The resulting 512×512 compressive sensing matrix is used to control the DMD mirror array. Two mirrors, M_1 and M_2, are adjusted to capture only half of the size of the DMD mirror array, thereby creating two corresponding matrices, Φ_1 and Φ_2, each with dimensions of 256×512. These two matrices are used for the compressive sensing of individual images coming from O_1 and O_2 through the optical system described in Figure 1. Five pairs of drone images were used, as shown in Figure 5, to evaluate the proposed model. Images from 1 to 5 represent O_1, and images from 6 to 10 represent O_2. Figures 6, 7, and 8 show the PSNR, NRMSE, and processing time values of the images when using the proposed matrix and the Gaussian and Bernoulli matrices. The results show that the proposed matrix outperforms the Gaussian and Bernoulli matrices in terms of PSNR and NRMSE, achieving higher reconstruction quality with lower error rates. Moreover, the recovery time for the proposed matrix remains competitive, ensuring efficient image reconstruction while maintaining good accuracy.

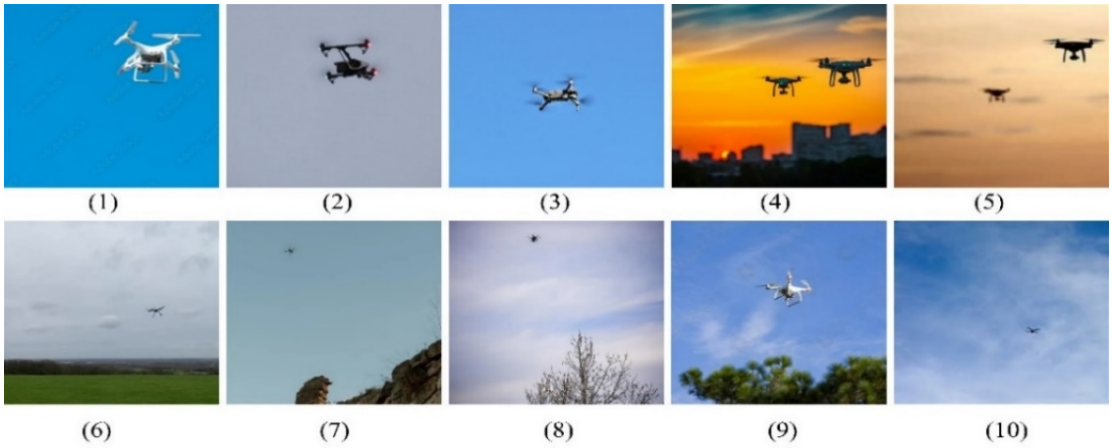

Fig. 5. Drone images used in the simulation.

TABLE I. SIMULATION PSNR, NRMSE, RECONSTRUCTION TIME VALUES

Image No.	PSNR (dB)			NRMSE			Time (s)		
	Gaussian	Bernoulli	Proposal	Gaussian	Bernoulli	Proposal	Gaussian	Bernoulli	Proposal
1	34.72	34.65	37.92	0.0413	0.0416	0.0285	2.3329	2.3402	1.9186
2	38.38	39.74	42.38	0.0183	0.0157	0.0115	1.937	1.8745	1.2893
3	34.59	34.07	37.44	0.0318	0.0337	0.0229	1.7181	1.5707	1.3103
4	32.9	32.59	35.67	0.0432	0.0448	0.0314	1.5832	1.5652	1.2227
5	40.44	39.68	43.95	0.0131	0.0143	0.0087	1.8549	1.923	1.4473
6	38.67	39.68	43.25	0.0174	0.0155	0.0103	1.992	2.0879	1.4517
7	32.32	32.13	34.68	0.0406	0.0416	0.0310	2.5428	2.7216	2.2042
8	22.45	22.43	24.52	0.1027	0.1030	0.0809	1.6356	1.6034	1.2834
9	33.83	33.48	36.46	0.0387	0.0376	0.0286	1.5686	1.5781	1.2402
10	49.95	49.05	52.39	0.0052	0.0058	0.0039	1.7603	1.7256	1.3771

TABLE II. COMPARISON OF THE PROPOSED SYSTEM WITH RELATED WORKS.

Studies	Method	FoV extension	Hardware complexity	Novelty/Drawback
[8, 9, 10]	Optical + AI	No	Medium	Narrow FoV limits detection area
[11, 12]	Optical + Acoustic	Partial extension	High (needs acoustic hardware)	The rotation mechanism slows the detection
[13]	CNN-based multi-FoV	Yes	Very high	Complex hardware and processing
This work	Optical + Compressive sensing + Binary matrix	Yes (2 FoVs)	Low (single sensor, no rotation)	Lightweight, fast, novel DMD control matrix

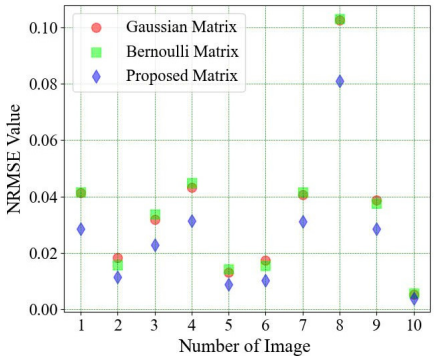

Fig. 6. PSNR of the reconstructed image

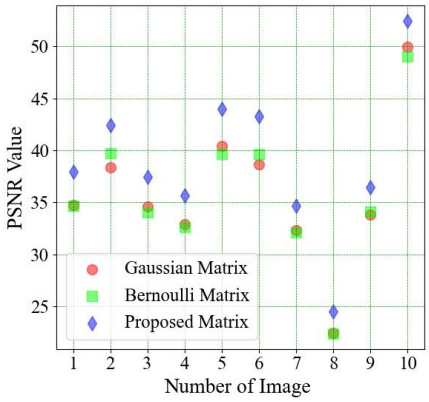

Fig. 7. NRMSE of the reconstructed image.

Table I presents the values of PSNR, NRMSE, and processing time in detail, respectively. The simulation results show that the drone image compressive sensing technique using the proposed matrix, along with the OMP restoration algorithm, achieved the highest PSNR value of 52.39 dB and the best NRMSE value of 0.004. The use of a binary matrix also makes the matrix generation and restoration process take the shortest time. In other words, PSNR, NRMSE, and processing time for the reconstruction images based on the proposed matrix are the best among the three methods. These values meet the standard required for most computer vision-based image processing systems. Table II shows a comparison between the proposed and existing systems in [10-13].

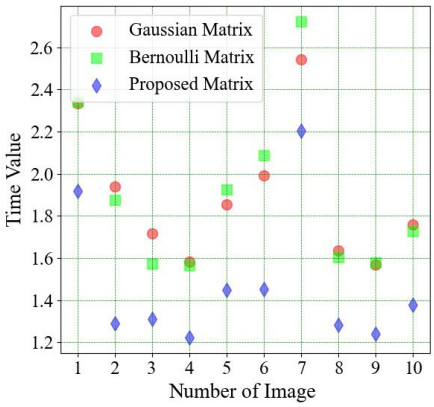

Fig. 8. Recovery time between cases.

V. CONCLUSIONS

This paper presents an optical model that applies compressive sensing techniques and utilizes the proposed DMD control matrix generation method. This is a novel and valuable feature of the system, as it allows the capture of images from two FoVs using a single 2D image sensor. The pseudorandom binary sequences generated by the proposed technique, which are columns of the DMD, have good characteristics in incoherence and capacity, due to the transformation of the sequence from linear to nonlinear. This condition ensures that the signal recovery process has as few errors as possible. The performance of the proposed DMD control matrix is better than two popular sampling matrices, Gaussian and Bernoulli. Using the proposed matrix significantly improves the quality of the reconstruction images

while significantly reducing hardware complexity and processing time. The maximum PSNR value reached 52.39 dB, and the NRMSE error value reached 0.0039 with only 50% sampling, which is better than previous works. In addition, the processing time is also the fastest compared to the other two matrices. The results of this work can be used to widen the FoV for optical-based drone detection systems. Future work will involve increasing the number of FoV and the development of an experimental system.

FUNDING

This research work was funded by the Electric Power University through a school-level scientific research project in 2023 (code: DTKHCN.11 2023).

REFERENCES

[1] M. Schneebeli *et al.*, "Drone detection with a multistatic C-band radar," in *2021 21st International Radar Symposium (IRS)*, Berlin, Germany, Jun. 2021, pp. 1–10, https://doi.org/10.23919/IRS51887.2021.9466200.

[2] P. Wellig *et al.*, "Radar Systems and Challenges for C-UAV," in *2018 19th International Radar Symposium (IRS)*, Bonn, Germany, Jun. 2018, pp. 1–8, https://doi.org/10.23919/IRS.2018.8448071.

[3] G. Fang, J. Yi, X. Wan, Y. Liu, and H. Ke, "Experimental Research of Multistatic Passive Radar With a Single Antenna for Drone Detection," *IEEE Access*, vol. 6, pp. 33542–33551, 2018, https://doi.org/10.1109/ACCESS.2018.2844556.

[4] S. Al-Emadi and F. Al-Senaid, "Drone Detection Approach Based on Radio-Frequency Using Convolutional Neural Network," in *2020 IEEE International Conference on Informatics, IoT, and Enabling Technologies (ICIoT)*, Doha, Qatar, Feb. 2020, pp. 29–34, https://doi.org/10.1109/ICIoT48696.2020.9089489.

[5] B. Kang, H. Ahn, and H. Choo, "A Software Platform for Noise Reduction in Sound Sensor Equipped Drones," *IEEE Sensors Journal*, vol. 19, no. 21, pp. 10121–10130, Aug. 2019, https://doi.org/10.1109/JSEN.2019.2927370.

[6] M. Ohlenbusch, A. Ahrens, C. Rollwage, and J. Bitzer, "Robust Drone Detection for Acoustic Monitoring Applications," in *2020 28th European Signal Processing Conference (EUSIPCO)*, Amsterdam, Netherlands, Jan. 2021, pp. 6–10, https://doi.org/10.23919/Eusipco47968.2020.9287433.

[7] F. Svanstrom, C. Englund, and F. Alonso-Fernandez, "Real-Time Drone Detection and Tracking With Visible, Thermal and Acoustic Sensors," in *2020 25th International Conference on Pattern Recognition (ICPR)*, Milan, Italy, Jan. 2021, pp. 7265–7272, https://doi.org/10.1109/ICPR48806.2021.9413241.

[8] P. Tang, C. Wang, X. Wang, W. Liu, W. Zeng, and J. Wang, "Object Detection in Videos by High Quality Object Linking," *IEEE Transactions on Pattern Analysis and Machine Intelligence*, vol. 42, no. 5, pp. 1272–1278, Feb. 2020, https://doi.org/10.1109/TPAMI.2019.2910529.

[9] Z. Q. Zhao, P. Zheng, S. T. Xu, and X. Wu, "Object Detection With Deep Learning: A Review," *IEEE Transactions on Neural Networks and Learning Systems*, vol. 30, no. 11, pp. 3212–3232, Aug. 2019, https://doi.org/10.1109/TNNLS.2018.2876865.

[10] O. Sahin and S. Ozer, "YOLODrone: Improved YOLO Architecture for Object Detection in Drone Images," in *2021 44th International Conference on Telecommunications and Signal Processing (TSP)*, Brno, Czech Republic, Jul. 2021, pp. 361–365, https://doi.org/10.1109/TSP52935.2021.9522653.

[11] F. Christnacher *et al.*, "Optical and acoustical UAV detection," in *Electro-Optical Remote Sensing X*, Oct. 2016, vol. 9988, pp. 83–95, https://doi.org/10.1117/12.2240752.

[12] S. Ding, X. Guo, T. Peng, X. Huang, and X. Hong, "Drone Detection and Tracking System Based on Fused Acoustical and Optical Approaches," *Advanced Intelligent Systems*, vol. 5, no. 10, 2023, Art. no. 2300251, https://doi.org/10.1002/aisy.202300251.

[13] M. Qiao, X. Liu, and X. Yuan, "Snapshot spatial–temporal compressive imaging," *Optics Letters*, vol. 45, no. 7, pp. 1659–1662, Apr. 2020, https://doi.org/10.1364/OL.386238.

[14] S. A-qian *et al.*, "Optical scanning holography based on compressive sensing using a digital micro-mirror device," *Optics Communications*, vol. 385, pp. 19–24, Feb. 2017, https://doi.org/10.1016/j.optcom.2016.10.034.

[15] W. Lu, T. Dai, and S. T. Xia, "Binary Matrices for Compressed Sensing," *IEEE Transactions on Signal Processing*, vol. 66, no. 1, pp. 77–85, Jan. 2018, https://doi.org/10.1109/TSP.2017.2757915.

[16] J. A. Tropp and A. C. Gilbert, "Signal Recovery From Random Measurements Via Orthogonal Matching Pursuit," *IEEE Transactions on Information Theory*, vol. 53, no. 12, pp. 4655–4666, Sep. 2007, https://doi.org/10.1109/TIT.2007.909108.

[17] M. Ebrahim, S. H. Adil, and D. Nawaz, "A Performance Comparative Analysis of Block Based Compressive Sensing and Line Based Compressive Sensing," *Engineering, Technology & Applied Science Research*, vol. 8, no. 2, pp. 2809–2813, Apr. 2018, https://doi.org/10.48084/etasr.1946.

[18] S. Vaucher, N. Yazdani, P. Felber, D. E. Lucani, and V. Schiavoni, "ZipLine: in-network compression at line speed," in *Proceedings of the 16th International Conference on emerging Networking EXperiments and Technologies*, Barcelona Spain, Nov. 2020, pp. 399–405, https://doi.org/10.1145/3386367.3431302.

[19] D. Datta, B. Datta, and H. S. Dutta, "Design and implementation of multibit LFSR on FPGA to generate pseudorandom sequence number," in *2017 Devices for Integrated Circuit (DevIC)*, Kalyani, India, Mar. 2017, pp. 346–349, https://doi.org/10.1109/DEVIC.2017.8073966.

[20] Q. L. Chi, C. N. Le, and T. P. Xuan, "A Hardware Oriented Method to Generate and Evaluate Nonlinear Interleaved Sequences with Desired Properties," *Journal of Information Engineering and Applications*, vol. 6, no. 7, 2016.

[21] L. C. Nguyen, V. K. Tran, and C. Q. Le, "On the Desired Properties of Linear Feedback Shift Register (LFSR) Based High-Speed PN-Sequence-Generator," in *Machine Learning for Predictive Analysis*, 2021, pp. 191–201, https://doi.org/10.1007/978-981-15-7106-0_19.

[22] S. G. Mallat and Z. Zhang, "Matching pursuits with time-frequency dictionaries," *IEEE Transactions on Signal Processing*, vol. 41, no. 12, pp. 3397–3415, Sep. 1993, https://doi.org/10.1109/78.258082.

[23] D. Needell and J. A. Tropp, "CoSaMP: Iterative signal recovery from incomplete and inaccurate samples," *Applied and Computational Harmonic Analysis*, vol. 26, no. 3, pp. 301–321, May 2009, https://doi.org/10.1016/j.acha.2008.07.002.

[24] J. Yang and Y. Zhang, "Alternating Direction Algorithms for l_1-Problems in Compressive Sensing," *SIAM Journal on Scientific Computing*, vol. 33, no. 1, pp. 250–278, Jan. 2011, https://doi.org/10.1137/090777761.

[25] H. Wang, F. Nie, and H. Huang, "Robust Distance Metric Learning via Simultaneous L1-Norm Minimization and Maximization," in *Proceedings of the 31st International Conference on Machine Learning*, Jun. 2014, pp. 1836–1844.

[26] Y. Arjoune, N. Kaabouch, H. El Ghazi, and A. Tamtaoui, "A performance comparison of measurement matrices in compressive sensing," *International Journal of Communication Systems*, vol. 31, no. 10, 2018, Art. no. e3576, https://doi.org/10.1002/dac.3576.